water

MDPI

Article

Cotransport of Cu with Graphene Oxide in Saturated Porous Media with Varying Degrees of Geochemical Heterogeneity

Jianzhou He [1], Dengjun Wang [2,*], Tingting Fan [1,3] and Dongmei Zhou [1,4,*]

1 Key Laboratory of Soil Environment and Pollution Remediation, Institute of Soil Science, Chinese Academy of Sciences, Nanjing 210008, China; hejianzh@msu.edu (J.H.); fantingting@nies.org (T.F.)
2 Oak Ridge Institute for Science and Education (ORISE) Resident Research Associate at the U.S. Environmental Protection Agency (EPA), Ada, OK 74820, USA
3 Nanjing Institute of Environmental Science, Ministry of Ecology and Environment of the People's Republic of China, Nanjing 210042, China
4 State Key Laboratory of Pollution Control & Resource Reuse, School of Environment, Nanjing University, Nanjing 210023, China
* Correspondence: wang.dengjun@epa.gov (D.W.); dmzhou@issas.ac.cn (D.Z.); Tel.: +1-(580)-436-8828 (D.W.); +86-25-86881180 (D.Z.); Fax: +1-(580)-436-8703 (D.W.); +86-25-86881000 (D.Z.)

Received: 7 January 2020; Accepted: 5 February 2020; Published: 7 February 2020

Abstract: Graphene oxide (GO) is likely to encounter heavy metals due to its widespread use and inevitable release into the subsurface environment, where the ubiquitous presence of iron oxides (e.g., hematite) would affect their interaction and transport. The present study aimed to investigate the cotransport of GO (20 mg L^{-1}) and copper (0.05 mM $CuCl_2$) in the presence of varying degrees of geochemical heterogeneity represented by iron oxide-coated sand fractions (ω = 0-0.45) in water-saturated columns under environmentally relevant physicochemical conditions (1 mM KCl at pH 5.0-9.0). The Langmuir-fitted maximum adsorption capacity of Cu^{2+} by GO reached 137.6 mg g^{-1}, and the presence of 0.05 mM Cu^{2+} decreased the colloidal stability and subsequent transport of GO in porous media. The iron oxide coating was found to significantly inhibit the transport of GO and Cu-loaded GO in sand-packed columns, which can be explained by the favorable deposition of the negatively charged GO onto patches of the positively charged iron oxide coatings at pH 5.0. Increasing the solution pH from 5.0 to 9.0 promoted the mobility of GO, with the exception of pH 7.5, in which the lowest breakthrough of GO was observed. This is possibly due to the fact that the surface charge of iron oxide approaches zero at pH 7.5, suggesting that new "favorable" sites are available for GO retention. This study deciphered the complicated interactions among engineered nanomaterials, heavy metals, and geochemical heterogeneity under environmentally relevant physicochemical conditions. Our results highlight the significant role of geochemical heterogeneity, such as iron oxide patches, in determining the fate and transport of GO and GO-heavy metal association in the subsurface environment.

Keywords: graphene oxide; copper; cotransport; porous media; and heterogeneity

1. Introduction

Graphene oxide (GO) is composed of hexagonal carbon sheets with abundant oxygen-containing functional groups (e.g., carboxyl, epoxy, and hydroxyl) on the basal and edge planes [1,2]. In recent years, GO has been promisingly used as a highly efficient adsorbent for heavy metal removal from water [3–6]. Evidence has shown that the adsorption capacity of GO is remarkedly higher than that of conventional adsorbents, such as activated carbon and other carbonaceous nanomaterials [4,7],

which is mainly attributable to electrostatic attraction and surface complexation of metal ions with the oxygen-containing functional groups of GO [5,8]. For example, the reported maximum adsorption capacity of Cu^{2+} on GO at pH 5.0 was 294 mg g^{-1} [5]. In addition, extensive studies have reported high mobility, transport, and release of GO in porous media [9–15]. These findings collectively raised a newly emerging concern that GO could potentially facilitate the transport of heavy metals through the subsurface environment via colloid-facilitated transport of contaminants [16,17].

The facilitated transport of heavy metals by GO has received considerable attention recently [15,18–21]. For instance, Zhou et al. [15] investigated the effects of GO concentration and solution ionic strength (IS) on the transport of Cu^{2+} in porous media. The authors reported that Cu^{2+} transport increased with increasing GO concentration (0-120 mg L^{-1}) and decreasing IS (1000-1 mM). Additionally, GO can promote the remobilization of pre-sorbed Pb^{2+} and Cd^{2+} in humic acid-, kaolinite-, and ferrihydrite-coated sand media; whereas no release of Pb^{2+}/Cd^{2+} was observed for smectite-coated sand columns [18,21]. Additionally, Zhang et al. [20] revealed that the enhanced transport of Pb^{2+} was due to the stripped oxidative debris from the surface of GO, which had greater mobility than the GO itself. However, little is known about how the ubiquitous presence of iron (hydro)oxides, representative of natural geochemical heterogeneity in soil and sediment aquifers, mediates the cotransport of GO with heavy metals (e.g., Cu). This knowledge gap will hinder our capacity to assess the hazard and risk of GO-facilitated transport of heavy metals in the subsurface.

Geochemical heterogeneities, such as the formation of biofilms or iron oxides on collector surfaces, have been demonstrated to significantly impact the transport and retention of GO and other engineered nanomaterials in porous media [9–11,22–24]. In our previous studies, biofilms developed from bacteria *Bacillus subtilis* and *Pseudomonas putida* were found to significantly inhibit the transport of GO by increasing the surface roughness and reducing the porosity and pore size in quartz sand columns. Unlike biofilms, iron oxide is amphoteric with a relatively high pH of point of zero charge (pH_{PZC} = 7.5) [25]. Hence, at an ambient pH in soil and sediment aquifers (pH < pH_{PZC} of iron oxide), the patches of iron oxides carry a positive surface charge and create "favorable" retention sites for negatively charged GO. Conversely, under alkaline pH conditions, the reversal of the surface charge of iron oxides can lead to an increase in the mobility of GO. To the best of our knowledge, limited investigation has been done on the cotransport of Cu with GO, especially with regard to solution pH change and the presence of geochemical heterogeneity.

The main objective of this work was to examine the cotransport of Cu with GO in water-saturated sand columns packed with mixtures of iron oxide-coated and uncoated sand grains at a wide pH range of 5.0-9.0. A two-site kinetic retention model was used to capture the transport behaviors of GO in porous media with varying degrees of geochemical heterogeneity. The findings of our research will help to better understand the fate, transport, and potential risk of GO-Cu complexes in the subsurface environment where geochemical heterogeneities like iron oxide patches occur.

2. Materials and Methods

2.1. Packed Sand Grains

Quartz sand (600-710 μm, Sinopharm Chemical Reagent Co., Ltd., Shanghai, China) was utilized as packing media for the column transport experiments. Before use, the sand was cleaned thoroughly following a previously established method [9,10] to remove any metal oxides and clay impurities. Geochemical heterogeneity was introduced by coating iron (Fe) oxide on sand grains [22]. Briefly, 500 g of quartz sand was mixed with 87.5 mL of 0.17 M $Fe(NO_3)_3$, followed by adding 90 mL of 0.52 M NaOH with vigorous stirring for 30 min. Then, the mixture was placed in an oven at 105 °C for 3 days, during which stirring was periodically performed to prevent crust formation on sand surfaces. The Fe oxide-coated sand was washed with 1.0 mM HCl and 1.0 mM NaOH to remove any weakly bonded iron compounds. The coated Fe oxide was examined using scanning electron microscopy (SEM, Hitachi S-3400N, Tokyo, Japan) equipped with energy dispersive X-ray spectroscopy (EDS, Figure S1

in the Supplementary Materials) and X-ray photoelectron spectroscopy (XPS, PHI 5000 VersaProbe, Chigasaki, Japan). The XPS results showed that the coated Fe oxide was hematite (α-Fe_2O_3, data not shown). Different Fe oxide fractions (ω, Table 1) in the column transport experiments were achieved by mixing the coated and uncoated sands [22]. The zeta potentials of sand colloids (ζ_{sand}) and Fe oxide coatings ($\zeta_{Fe\ oxides}$) were determined by a NanoBrook 90Plus PALS Analyzer (Brookhaven, NY, USA). Furthermore, a relationship between the overall ζ-potential of chemically heterogeneous collectors (ζ_C, Table 1), the ζ_{sand}, and the $\zeta_{Fe\ oxides}$ was used to calculate the variation of zeta potential with varying Fe oxide fractions ω [22,26]. Details were given in Text S1 of the Supplementary Materials.

2.2. Graphene Oxides

Graphene oxide (GO, purity >99%) was purchased from the Nanjing XFNANO Materials Tech Co., Ltd. (Nanjing, China). The received GO stock solution (2.0 mg mL^{-1}) was dispersed in deionized (DI) water and stored at 4 °C [10]. The Cu-loaded GO suspension was prepared by introducing aliquots of GO stock solution into 1 mM KCl and 0.05 mM $CuCl_2$, and the solution pH was adjusted to 5.0 ± 0.2 using 0.1 mM HCl and/or KOH. The resulting suspension was then sonicated at 45 kHz and 100 W (KQ-300VDE, Kunshan Sonicator Co., Shanghai, China) for 1 h before use. The zeta potential (ζ) and hydrodynamic diameter (D_h) of GO and Cu-loaded GO suspensions were measured with the NanoBrook 90Plus PALS shown above.

2.3. Adsorption of Cu on Graphene Oxides

The batch adsorption experiments of Cu^{2+} on GO were performed at pH 5.0 and in 1 mM KCl at room temperature. In brief, aliquots of GO stock suspension were mixed with $CuCl_2$ in 50-mL conical centrifuge tubes. The resultant solutions contained 500 mg L^{-1} of GO and varying concentrations of Cu^{2+} at 0, 0.05, 0.1, 0.2, 0.4, 0.6, 0.8, and 1.0 mM. All experiments were conducted in duplicate. The centrifuge tubes were continuously shaken at 200 rpm, at 25 °C in the dark for 20 h to reach equilibrium [4,5]. Then the reaction solutions were centrifuged at 11,000× *g* for 30 min and filtered through 0.22-µm membrane filters (Supplementary Materials Text S2 and Figure S2). The dissolved Cu^{2+} in the filtrate was determined using atomic absorption spectrophotometry (AAS, Hitachi Z-2000, Tokyo, Japan). The Cu adsorbed on GO was calculated as the difference between the total and dissolved Cu concentrations. The adsorption isotherm was fitted with the Langmuir model (Text S3 and Figure 1).

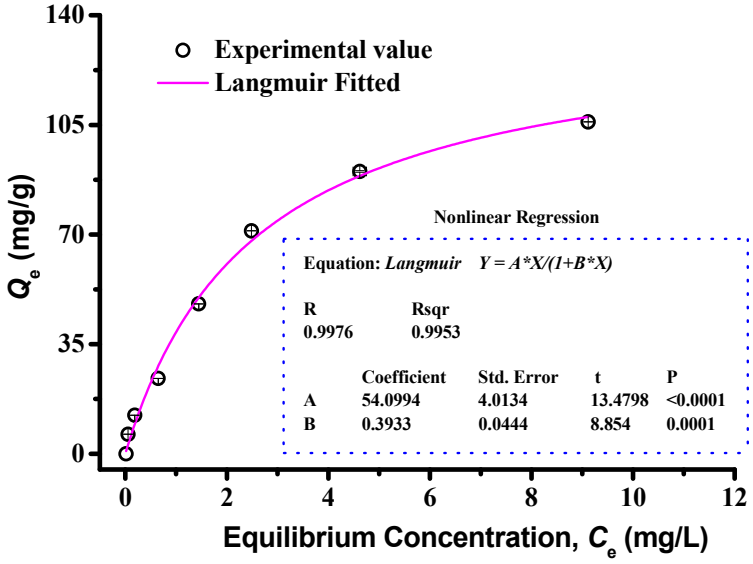

Figure 1. Langmuir isotherm for Cu^{2+} adsorption on 500 mg L^{-1} of GO at pH 5.0 and 1 mM KCl.

2.4. Column Transport Experiments

Three sets of column experiments were conducted to investigate the transport of GO and Cu-loaded GO in the presence of geochemical heterogeneity (Table 1). The first set examined the role of surface charge heterogeneity in the form of Fe oxide-coated sand fractions (ω = 0, 0.15, 0.30, and 0.45) on the transport behaviors of GO in saturated porous media. The second experiment was designed to explore the effect of solution pH (5.0, 6.3, 7.5, and 9.0) on GO transport when ω = 0.30. A third set of experiments investigated the cotransport of Cu with GO in saturated columns packed with varying fractions of Fe oxide-coated sands.

Glass chromatography columns (2.6-cm diameter × 20-cm height, Shanghai Huxi Glassware Co., Shanghai, China) were dry-packed with uncoated and Fe oxide-coated sand mixtures. The packed media were supported by 80-μm stainless steel mesh on both ends. In the following step, the column was saturated and conditioned by sequential injection of DI water and 1 mM KCl background solution in an upward direction at a constant flow rate of 1.0 mL min^{-1} for several hours using a peristaltic pump (YZΠ-15, Baoding Longer Precision Pump Co., Ltd., Baoding, China). The porosity of packed columns was 0.42 determined gravimetrically.

The working GO influents (20 mg L^{-1}) with or without 0.05 mM of Cu^{2+} were injected for 4.0 pore volumes (PVs) at an identical flow rate, followed by introducing 3.5 PV of background solution (i.e., 1 mM KCl). The column effluents were collected at predetermined time intervals using a fraction collector ((BS-100A, Huxi Analytical Instrument Factory Co., Ltd., Shanghai, China). The concentration of GO in the effluent was analyzed spectrophotometrically (721-100, Shanghai, China) at the optimal wavelength of 228 nm [9,10]. For cotransport experiments, aliquots (5 mL) of outflow solutions were centrifuged (11,000× *g*, 30 min) and filtered through a 0.22-μm membrane filter to measure the dissolved Cu concentration in the filtrates using AAS, as described above and in Text S2 of the Supplementary Materials. The GO facilitated (GO-F) Cu was calculated by the difference between the total and dissolved Cu^{2+} ions. All breakthrough curves (BTCs) of GO were plotted as normalized effluent concentrations (C/C_0) as a function of injected pore volumes (PVs).

2.5. Numerical Modeling

In the present study, the pore–water velocity and longitudinal dispersity of packed column were obtained by fitting tracer BTCs using the CXTFIT code [27]. The convection–dispersion equation with two kinetic retention sites [28,29] was used to describe the experimental BTCs of GO and Cu-loaded GO in saturated porous media. It is assumed that the first site is reversible using the first-order retention rate coefficient (k_{1d}) and detachment rate coefficient (k_{1det}), while the second site is irreversible and accounted by the first-order retention rate coefficient (k_{2d}) and a Langmuirian dynamic blocking function [30]. The HYDRUS-1D code [31] was applied to numerically estimate the transport parameters of GO and Cu-loaded GO by inverse fitting the experimentally observed BTCs with a non-linear least square optimization routine based on the Levenberg–Marquardt algorithm [32]. A detailed description on the model equations of the two-site kinetic retention model can be found in our previous work [9,10,22] and in Text S4 of the Supplementary Materials.

3. Results and Discussion

3.1. Properties of GO and Sand Media

Table 1 presents the electrokinetic properties of GO and quartz sand at different pH and 1 mM KCl. The ζ-potentials of GO and collectors were negative and decreased progressively in response to the increase of solution pH (5.0-9.0). This is due to the dissociation of protons on GO and sand surfaces [22,33]. Correspondingly, the hydrodynamic diameters (D_h) of GO decreased from 960 nm to 785 nm, which is ascribed to the enhancement of electrostatic repulsion between GO particles as pH increase. With the addition of 0.05 mM Cu^{2+}, the ζ-potential and D_h of GO increased to −22.7 mV and 1045 nm, respectively, indicative of a lower stability of GO. This can be explained by the fact that surface

complexation of Cu^{2+} with oxygen-containing functional groups (e.g., -OH and -COOH) of GO tended to decrease the GO dispersibility [5,34]. Sitko et al. [5] also observed pronounced agglomeration and precipitation of GO after adsorption of Cu^{2+}, Zn^{2+}, Cd^{2+}, and Pb^{2+}. This finding suggests that metal ions (e.g., Cu^{2+}) may change the dispersity and subsequent transport behavior of GO in subsurface environments. As per our previous studies [22,26], a linear relationship was used to calculate the overall zeta potentials of the collectors (ζ_C, mixture of uncoated and Fe oxide-coated sands, Table 1 and Text S1). The value of ζ_C became less negative as the fraction of Fe oxides in sand columns increased (ω = 0-0.45). It is expected that geochemical heterogeneities would have a notable impact on the transport of GO and cotransport of Cu with GO.

Table 1. Summarized experimental setups, properties of GO and quartz sand, and fitted model parameters.

Setup	ω	pH	Cu^{2+} (mM)	D_h (nm)	ζ_{GO} (mV)	ζ_C (mV)	k_{1d}	k_{1det}	k_{2d}	S_{max2}/C_0	R^2
Fe oxide fractions (Figure 2)	0	5.0	0	960	−39.7	−25.7	2.69	2.19	0.01	0.03	0.999
	0.15	5.0	0	960	−39.7	−20.5	2.94	2.26	0.05	0.42	0.998
	0.30	5.0	0	960	−39.7	−15.3	1.11	0.96	0.06	0.90	0.991
	0.45	5.0	0	960	−39.7	−10.2	3.83	3.23	0.05	1.16	0.994
pH changes (Figure 3)	0.30	5.0	0	960	−39.7	−15.3	1.11	0.96	0.06	0.90	0.991
	0.30	6.3	0	922	−40.9	−29.6	2.74	1.85	0.04	0.61	0.998
	0.30	7.5	0	869	−43.6	−41.2	1.44	1.03	0.06	1.36	0.990
	0.30	9.0	0	785	−46.8	−53.4	1.56	1.04	0.01	0.40	0.999
Cotransport (Figure 4)	0	5.0	0.05	1045	−22.7	−25.7	1.62	1.31	0.03	0.33	0.999
	0.15	5.0	0.05	1045	−22.7	−20.5	1.22	0.94	0.05	0.91	0.996
	0.30	5.0	0.05	1045	−22.7	−15.3	1.86	1.16	0.06	1.21	0.996
	0.45	5.0	0.05	1045	−22.7	−10.2	0.70	0.72	0.06	1.18	0.995

D_h represents the averaged hydrodynamic diameter of GO as measured by dynamic light scattering; ζ_{GO} and ζ_{tot} are zeta potentials of GO and collectors, respectively; k_{1d} and k_{1det} are the first-order retention and detachment rate coefficient on site 1, respectively; k_{2d} is the first-order retention rate coefficient on site 2; S_{max2} is maximum solid-phase retained concentration of GO on site 2; R^2 is Pearson's correlation coefficient.

3.2. Adsorption Isotherm of Cu on GO

At pH = 5.0 and IS = 1.0 mM KCl, the adsorption isotherm of Cu^{2+} on GO is shown in Figure 1. The amount of Cu adsorbed onto GO was observed to increase as the aqueous Cu concentration increased. The Langmuir adsorption model successfully fitted the isotherm data with $R^2 > 0.995$, indicating a monolayer adsorption of Cu on the surface of GO. The simulated maximum amount (Q_{max}) was 137.6 mg g^{-1}, which agrees with the literature reported values of 46.6~294 mg g^{-1} [4,5]. The high adsorption capacity resulted from the large specific surface area (90.3 m^2 g^{-1}, as determined using the BET method), although this number is dramatically lower than the theoretical BET surface area (2700 m^2 g^{-1}) of monolayered GO, which could be ascribed to the aggregation and stacking of GO flakes [35]. On the other hand, the high value of Q_{max} suggests that adsorption of Cu on GO is controlled dominantly by chemisorption, such as surface complexation with oxygen-containing functional groups (e.g., carbonyl and hydroxyl on the basal plane and carboxyl on the edge) [2,5].

3.3. Role of Chemical Heterogeneity

Figure 2 depicts the role of surface charge heterogeneity as introduced by various mixtures of uncoated and Fe oxide-coated sands (ω = 0, 0.15, 0.30, and 0.45) on the transport of GO at pH = 5.0 and IS = 1.0 mM KCl. A considerably high mobility of GO was observed in the saturated column, and the Fe oxide fraction significantly hindered GO transport, e.g., the breakthrough of GO was retarded and the normalized effluent concentration (which is expressed as C/C_0) declined accordingly with the increase of Fe oxide fractions (ω). For example, the value of C/C_0 reduced from ~1.0 to 0.75 as ω increased from 0 to 0.45. This is because under experimental pH 5.0, which is lower than the pH of

point of zero charge (pH_{PZC} = 7.5) of Fe oxide [25], a certain fraction of sand surface was favorable for the deposition of the negatively charged GO (Table 1). Particularly, the amounts of retained GO and the breakthrough time it took for GO to fill these favorable sites were correlated with the Fe oxide surface areas (i.e., ω).

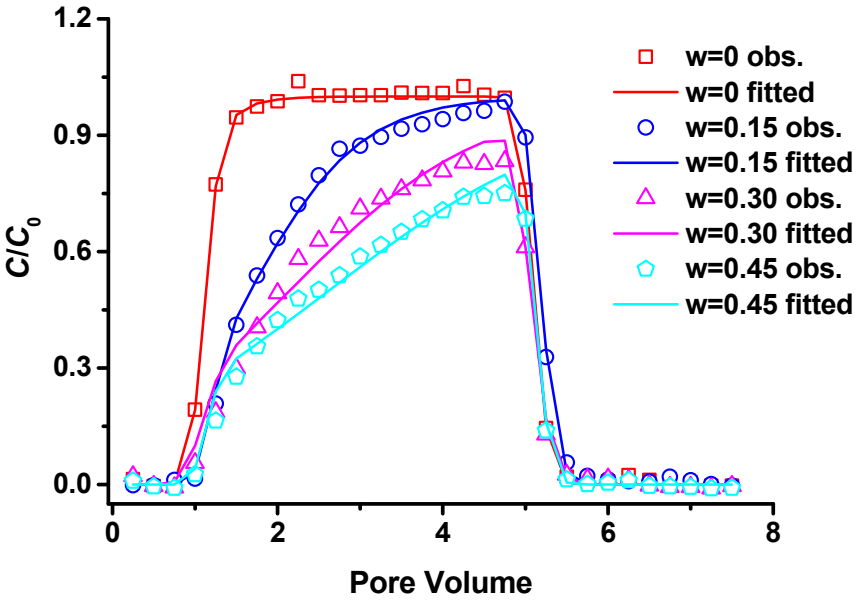

Figure 2. Observed (dots) and simulated (solid lines) breakthrough curves (BTCs) of GO under different Fe oxide fractions (ω = 0-0.45) at pH = 5.0 and IS = 1.0 mM KCl. Symbols are experimental data and solid lines are the fitted results obtained from the two-site kinetic attachment model.

Table 1 gives the model-fitted parameters of k_{1d}, k_{1det}, k_{2d}, S_{max2}/C_0, and the correlation coefficients (R^2). The two-site kinetic retention model simulated the BTCs of GO well at all investigated experimental conditions with an $R^2 > 0.99$. A Langmuirian blocking function on site 2 that accounted for the surface charge heterogeneity (i.e., Fe oxide fraction) of porous media was used to explain the irreversible retention of GO on sand collectors. The first-order retention rate coefficient (k_{1d}) and detachment rate coefficient (k_{1det}) were not a function of Fe oxide fractions ω, which implies that k_{1d} and k_{1det} are not sensitive to the change of ω. In comparison, the value of k_{2d} and S_{max2}/C_0 increased with ω, confirming the model assumption and suggesting that k_{2d} was mainly governed by the surface chemical heterogeneity. Note that k_{2d} and S_{max2} values were proportional to the patchy or inhomogeneous surface coatings, as is well documented in previous literature [10,22,26,36].

3.4. Effect of Solution pH

The surface charge of Fe oxide and GO would change as a function of solution pH, thereby affecting GO attachment behavior. Figure 3 shows the observed and simulated BTCs of GO under various solution pH (5.0-9.0) at IS = 1 mM KCl and in the presence of geochemical heterogeneity (ω = 0.30). Collectively, the mobility of GO increased as solution pH increased, which is attributed to the opposite electrostatic conditions, which are expected to be favorable at low pH (5.0 and 6.3) and unfavorable at high pH (9.0) for GO attachment. Intriguingly, the lowest normalized effluent concentration (C/C_0 = 0.70) was noticed when pH = 7.5. The possible explanation is that Fe oxides are amphoteric minerals with a pH_{PZC} of 7.5, under this pH condition, the surface charge of Fe oxides is close to zero, where new "favorable" retention sites are available for GO deposition.

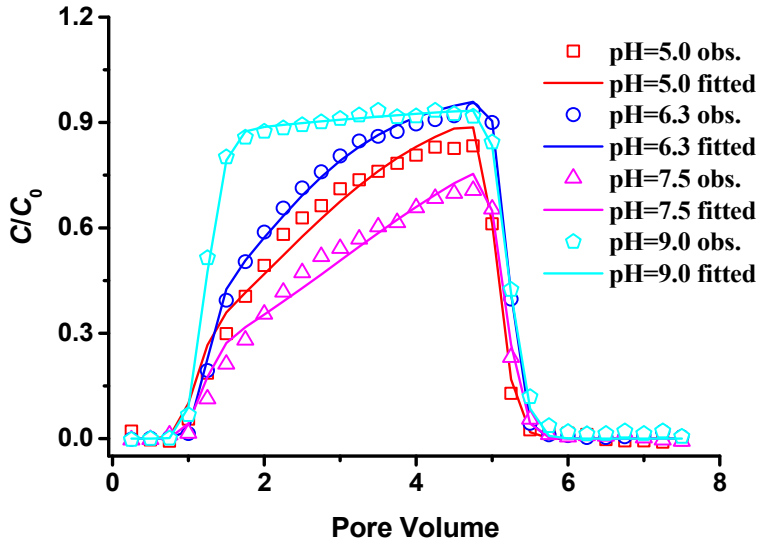

Figure 3. Observed (dots) and simulated (solid lines) breakthrough curves (BTCs) of GO at different solution pH as ω = 0.30 and IS = 1.0 mM KCl. Symbols are experimental data and solid lines are the fitted results obtained from the two-site kinetic attachment model.

More importantly, this exception was successfully captured by the two-site kinetic retention model ($R^2 > 0.99$). The fitted parameters of k_{2d} and S_{max2}/C_0 were 0.06 and 1.36, respectively, which were significantly larger than that obtained from other experimental conditions (pH = 5.0, 6.3, and 9.0, Table 1). Again, the k_{1d} and k_{1det} values on site 1 were relatively insensitive to the change in solution pH, which emphasizes these two parameters were presumably controlled by the hydrodynamics. Wang et al. [22] found that the value of k_{1d} and k_{1det} increased with increasing pore–water flow velocity.

3.5. Cotransport of Cu with GO

The cotransport of Cu^{2+} with GO was examined under different Fe oxide fractions (ω = 0–0.45) at pH 5.0 and IS = 1 mM KCl, as shown in Figure 4. A similar transport pattern (i.e., the normalized concentration (C/C_0) declined with an increase of ω) but a relatively lower mobility of Cu-loaded GO was observed in comparison to that of only GO (Figure 2). This is because the presence of Cu^{2+} increased the ζ-potential (less negative) and the hydrodynamic diameter (D_h) of GO (Table 1), and subsequently reduced GO transport in porous media, which is in accordance with the literature [18,21]. Likewise, Qi et al. [37] demonstrated that Cu^{2+} ions increased the aggregation of GO, thereby generally increasing the transport–enhancement capability of GO. In the presence of GO, the breakthrough of total (Figure S3a), dissolved (Figure S3b), and GO-facilitated (GO-F) Cu (Figure 4b) followed the same trend, exhibiting decreased migration and even retardant behavior as ω increased from 0 to 0.45, compared to sole Cu^{2+} transport in the column (Figure S4). These trends were due to enhanced retention of GO with varying degrees of geochemical heterogeneity. Increasing ω reduced the concentrations of total, dissolved, and GO-F Cu in the effluents, which indicates that the Fe oxide coatings had strongly high adsorption capacities for Cu [22,38]. For example, the amount of Cu associated with concurrent GO in the influents was 0.99 mg L^{-1}, accounting for 25.3% of total Cu, whereas decreased to 0.84 mg L^{-1} (21.5%) when ω = 0 and further to 0.57 mg L^{-1} (14.6%) when ω = 0.45 in the effluents. Zhou et al. [15] disclosed that GO had a higher adsorption affinity for Cu^{2+} ions than quartz sand did, which led to complexation of GO with pre-adsorbed Cu from sand surface and served as an effective carrier. This is consistent with the findings of Jiang et al. [18], that the high affinity of GO for Pb^{2+} and Cd^{2+} ions presorbed on sands resulted in their remobilization and cotransport through sand columns. To this regard, our observations suggest that some Cu was dissociated from GO surface during the cotransport process, which facilitates their irreversible deposition on Fe oxide-coated sand grains.

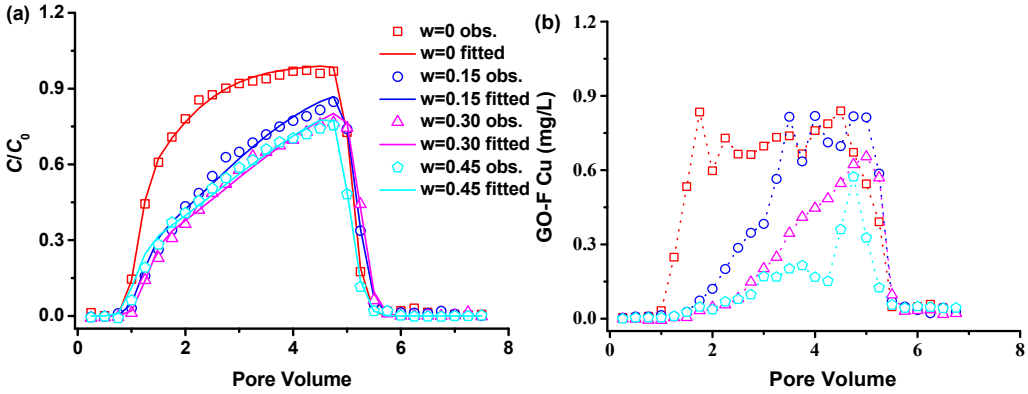

Figure 4. Observed (dots) and simulated (solid lines) transport of Cu-loaded GO (**a**) and observed (dots connected using dash lines) GO-facilitated Cu (**b**) under different Fe oxide fractions (ω = 0-0.45) at pH = 5.0 and IS = 1.0 mM KCl. Symbols are experimental data and solid lines are the fitted results obtained from the two-site kinetic attachment model, as shown in (**a**).

4. Conclusions

Iron oxides are common forms of geochemical heterogeneity ubiquitously present in natural soil and sediment aquifers with concentrations ranging from μg L^{-1} to mg L^{-1} [23,39]. Our results generated from this research demonstrated that the presence of iron oxide coatings significantly decreased the mobility of GO and Cu-loaded GO in water-saturated sand columns. Due to the fact that iron oxide is amphoteric with a $pH_{PZC} \approx 7.5$, solution pH changing from 5.0 to 9.0 was expected to increase the transport of GO in the presence of iron oxide coating (ω = 0.30). This is thought to be because of a switch from favorable attachment at a low pH (5.0 and 6.3) to unfavorable attachment at a high pH (9.0) for GO. The GO had a high adsorption capacity of 137.6 mg g^{-1} for Cu^{2+} ions. While Cu-loaded GO exhibited a lower transport potential due to decreased mobility. Please note that partial disassociation of Cu from GO surface occurred during the cotransport process. To better understand the significance of iron oxide on the fate and transport of contaminants (e.g., engineered nanomaterials and heavy metals) in subsurface environments, it is needed to incorporate more environmental factors such as wetting–drying, freezing–thawing, and redox conditions in future research.

Supplementary Materials: The following are available online at http://www.mdpi.com/2073-4441/12/2/444/s1, Figure S1: Selected SEM image of Fe oxide-coated quartz sand used in the study and the corresponding energy dispersive x-ray spectroscopy for elemental composition analysis; Figure S2. Method comparison for separating dissolved Cu^{2+} from bulk solution in the presence of 20 mg L^{-1} GO; Figure S3. The total (a) and dissolved (b) concentrations of Cu in the effluents as a function of Fe oxide fraction (ω) at pH 5.0 and 1 mM KCl; Figure S4. The breakthrough curve of 0.05 mM $CuCl_2$ in sand column (ω = 0) at pH 5.0 and 1 mM KCl.

Author Contributions: Conceptualization, J.H., D.W. and D.Z.; Methodology, J.H., D.W. and T.F.; Data curation, J.H. and T.F.; Writing – original draft, J.H.; Writing – review & editing, D.W., T.F. and D.Z.; Funding acquisition, D.Z.; Supervision, D.W. and D.Z. All authors have read and agreed to the published version of the manuscript.

Funding: This research was funded by the National Natural Science Foundation of China (41430752 and 41125007) and the National Key Research and Development Program of China (2017YFA0207001).

Acknowledgments: We acknowledge the help from Geoff Rhodes (Michigan State University) for improving the quality of this paper.

Conflicts of Interest: The authors declare no conflict of interest.

References

1. He, H.; Klinowski, J.; Forster, M.; Lerf, A. A new structural model for graphite oxide. *Chem. Phys. Lett.* **1998**, *287*, 53–56. [CrossRef]
2. Dreyer, D.R.; Park, S.; Bielawski, C.W.; Ruoff, R.S. The chemistry of graphene oxide. *Chem. Soc. Rev.* **2010**, *39*, 228–240. [CrossRef] [PubMed]

3. Wu, W.; Yang, Y.; Zhou, H.; Ye, T.; Huang, Z.; Liu, R.; Kuang, Y. Highly efficient removal of Cu(II) from aqueous solution by using graphene oxide. *Water Air Soil Pollut.* **2012**, *224*, 1372. [CrossRef]
4. Yang, S.-T.; Chang, Y.; Wang, H.; Liu, G.; Chen, S.; Wang, Y.; Liu, Y.; Cao, A. Folding/aggregation of graphene oxide and its application in Cu^{2+} removal. *J. Colloid Interface Sci.* **2010**, *351*, 122–127. [CrossRef]
5. Sitko, R.; Turek, E.; Zawisza, B.; Malicka, E.; Talik, E.; Heimann, J.; Gagor, A.; Feist, B.; Wrzalik, R. Adsorption of divalent metal ions from aqueous solutions using graphene oxide. *Dalton Trans.* **2013**, *42*, 5682–5689. [CrossRef]
6. Yu, J.-G.; Yu, L.-Y.; Yang, H.; Liu, Q.; Chen, X.-H.; Jiang, X.-Y.; Chen, X.-Q.; Jiao, F.-P. Graphene nanosheets as novel adsorbents in adsorption, preconcentration and removal of gases, organic compounds and metal ions. *Sci. Total Environ.* **2015**, *502*, 70–79. [CrossRef]
7. Sitko, R.; Zawisza, B.; Malicka, E. Modification of carbon nanotubes for preconcentration, separation and determination of trace-metal ions. *TrAC Trends Anal. Chem.* **2012**, *37*, 22–31. [CrossRef]
8. Machida, M.; Mochimaru, T.; Tatsumoto, H. Lead(II) adsorption onto the graphene layer of carbonaceous materials in aqueous solution. *Carbon* **2006**, *44*, 2681–2688. [CrossRef]
9. He, J.; Li, C.; Wang, D.; Zhou, D. Biofilms and extracellular polymeric substances mediate the transport of graphene oxide nanoparticles in saturated porous media. *J. Hazard. Mater.* **2015**, *300*, 467–474. [CrossRef]
10. He, J.; Wang, D.; Fang, H.; Fu, Q.; Zhou, D. Inhibited transport of graphene oxide nanoparticles in granular quartz sand coated with *Bacillus subtilis* and *Pseudomonas putida* biofilms. *Chemosphere* **2017**, *169*, 1–8. [CrossRef] [PubMed]
11. Wang, D.; Shen, C.; Jin, Y.; Su, C.; Chu, L.; Zhou, D. Role of solution chemistry in the retention and release of graphene oxide nanomaterials in uncoated and iron oxide-coated sand. *Sci. Total Environ.* **2017**, *579*, 776–785. [CrossRef] [PubMed]
12. Liu, L.; Gao, B.; Wu, L.; Morales, V.L.; Yang, L.; Zhou, Z.; Wang, H. Deposition and transport of graphene oxide in saturated and unsaturated porous media. *Chem. Eng. J.* **2013**, *229*, 444–449. [CrossRef]
13. Feriancikova, L.; Xu, S. Deposition and remobilization of graphene oxide within saturated sand packs. *J. Hazard. Mater.* **2012**, *235–236*, 194–200. [CrossRef] [PubMed]
14. Lanphere, J.D.; Luth, C.J.; Walker, S.L. Effects of solution chemistry on the transport of graphene oxide in saturated porous media. *Environ. Sci. Technol.* **2013**, *47*, 4255–4261. [CrossRef] [PubMed]
15. Zhou, D.D.; Jiang, X.H.; Lu, Y.; Fan, W.; Huo, M.X.; Crittenden, J.C. Cotransport of graphene oxide and Cu(II) through saturated porous media. *Sci. Total Environ.* **2016**, *550*, 717–726. [CrossRef]
16. McCarthy, J.F.; Zachara, J.M. Subsurface transport of contaminants. *Environ. Sci. Technol.* **1989**, *23*, 496–502. [CrossRef]
17. Wang, D.; Paradelo, M.; Bradford, S.A.; Peijnenburg, W.J.G.M.; Chu, L.; Zhou, D. Facilitated transport of Cu with hydroxyapatite nanoparticles in saturated sand: Effects of solution ionic strength and composition. *Water Res.* **2011**, *45*, 5905–5915. [CrossRef]
18. Jiang, Y.; Zhang, X.; Yin, X.; Sun, H.; Wang, N. Graphene oxide-facilitated transport of Pb^{2+} and Cd^{2+} in saturated porous media. *Sci. Total Environ.* **2018**, *631–632*, 369–376. [CrossRef]
19. Jiang, Y.; Yin, X.; Guan, D.; Jing, T.; Sun, H.; Wang, N.; Bai, J. Co-transport of Pb(II) and oxygen-content-controllable graphene oxide from electron-beam-irradiated graphite in saturated porous media. *J. Hazard. Mater.* **2019**, *375*, 297–304. [CrossRef]
20. Zhang, J.; Xie, X.; Meng, X.; Li, Y.; Zhu, W. Release and transport of Pb(II) adsorbed on graphene oxide under alkaline conditions in a saturated sand column. *J. Hazard. Mater.* **2019**, *377*, 357–364. [CrossRef]
21. Yin, X.; Jiang, Y.; Tan, Y.; Meng, X.; Sun, H.; Wang, N. Co-transport of graphene oxide and heavy metal ions in surface-modified porous media. *Chemosphere* **2019**, *218*, 1–13. [CrossRef] [PubMed]
22. Wang, D.; Bradford, S.A.; Paradelo, M.; Peijnenburg, W.J.G.M.; Zhou, D. Facilitated transport of copper with hydroxyapatite nanoparticles in saturated sand. *Soil Sci. Soc. Am. J.* **2012**, *76*, 375–388. [CrossRef]
23. Wang, D.; Zhang, W.; Zhou, D. Antagonistic effects of humic acid and iron oxyhydroxide grain-coating on biochar nanoparticle transport in saturated sand. *Environ. Sci. Technol.* **2013**, *47*, 5154–5161. [CrossRef]
24. Wang, D.; Bradford, S.A.; Harvey, R.W.; Gao, B.; Cang, L.; Zhou, D. Humic Acid Facilitates the Transport of ARS-Labeled Hydroxyapatite Nanoparticles in Iron Oxyhydroxide-Coated Sand. *Environ. Sci. Technol.* **2012**, *46*, 2738–2745. [CrossRef] [PubMed]
25. Parks, G.A. The isoelectric points of solid oxides, solid hydroxides, and aqueous hydroxo complex systems. *Chem. Rev.* **1965**, *65*, 177–198. [CrossRef]

26. Elimelech, M.; Nagai, M.; Ko, C.-H.; Ryan, J.N. Relative insignificance of mineral grain zeta potential to colloid transport in geochemically heterogeneous porous media. *Environ. Sci. Technol.* **2000**, *34*, 2143–2148. [CrossRef]
27. Toride, N.; Leij, F.; Van Genuchten, M.T. *The CXTFIT Code for Estimating Transport Parameters from Laboratory or Field Tracer Experiments*; Version 2.1; U.S. Salinity Laboratory, USDA-ARS: Riverside, CA, USA, 1999; Volume 2.
28. Bradford, S.A.; Simunek, J.; Bettahar, M.; van Genuchten, M.T.; Yates, S.R. Modeling colloid attachment, straining, and exclusion in saturated porous media. *Environ. Sci. Technol.* **2003**, *37*, 2242–2250. [CrossRef]
29. Schijven, J.F.; Šimůnek, J. Kinetic modeling of virus transport at the field scale. *J. Contam. Hydrol.* **2002**, *55*, 113–135. [CrossRef]
30. Adamczyk, Z.; Siwek, B.; Zembala, M.; Belouschek, P. Kinetics of localized adsorption of colloid particles. *Adv. Colloid Interface Sci.* **1994**, *48*, 151–280. [CrossRef]
31. Simunek, J.; Van Genuchten, M.T.; Sejna, M. The HYDRUS-1D software package for simulating the one-dimensional movement of water, heat, and multiple solutes in variably-saturated media. *Univ. Calif. Riverside Res. Rep.* **2005**, *3*, 1–240.
32. Marquardt, D.W. An algorithm for least-squares estimation of nonlinear parameters. *J. Soc. Ind. Appl. Math.* **1963**, *11*, 431–441. [CrossRef]
33. Elimelech, M.; Gregory, J.; Jia, X. *Particle Deposition and Aggregation: Measurement, Modelling and Simulation*; Butterworth-Heinemann: Oxford, UK, 1995.
34. Sun, Y.; Yang, S.; Chen, Y.; Ding, C.; Cheng, W.; Wang, X. Adsorption and desorption of U(VI) on functionalized graphene oxides: A combined experimental and theoretical study. *Environ. Sci. Technol.* **2015**, *49*, 4255–4262. [CrossRef] [PubMed]
35. Whitby, R.L.D.; Gun'ko, V.M.; Korobeinyk, A.; Busquets, R.; Cundy, A.B.; László, K.; Skubiszewska-Zięba, J.; Leboda, R.; Tombácz, E.; Toth, I.Y.; et al. Driving forces of conformational changes in single-layer graphene oxide. *ACS Nano* **2012**, *6*, 3967–3973. [CrossRef] [PubMed]
36. Bradford, S.A.; Kim, H.N.; Haznedaroglu, B.Z.; Torkzaban, S.; Walker, S.L. Coupled factors influencing concentration-dependent colloid transport and retention in saturated porous media. *Environ. Sci. Technol.* **2009**, *43*, 6996–7002. [CrossRef] [PubMed]
37. Qi, Z.; Hou, L.; Zhu, D.; Ji, R.; Chen, W. Enhanced transport of phenanthrene and 1-naphthol by colloidal graphene oxide nanoparticles in saturated soil. *Environ. Sci. Technol.* **2014**, *48*, 10136–10144. [CrossRef]
38. Weng, L.; Van Riemsdijk, W.H.; Hiemstra, T. Cu^{2+} and Ca^{2+} adsorption to goethite in the presence of fulvic acids. *Geochim. Cosmochim. Acta* **2008**, *72*, 5857–5870. [CrossRef]
39. Li, M.; He, L.; Zhang, M.; Liu, X.; Tong, M.; Kim, H. Cotransport and deposition of iron oxides with different-sized plastic particles in saturated quartz sand. *Environ. Sci. Technol.* **2019**, *53*, 3547–3557. [CrossRef]